

2009

Enhanced optical conductivity of bilayer graphene nanoribbons in the terahertz regime

Anthony Wright

University of Wollongong, arw75@uow.edu.au

Chao Zhang

University of Wollongong, chao_zhang@uow.edu.au

Juncheng Cao

University of Wollongong, null@uow.edu.au

Publication Details

Wright, A., Cao, J. & Zhang, C. (2009). Enhanced optical conductivity of bilayer graphene nanoribbons in the terahertz regime. *Physical Review Letters*, 103 (20), 207401-1-207401-4.

Enhanced Optical Conductivity of Bilayer Graphene Nanoribbons in the Terahertz Regime

A. R. Wright,¹ J. C. Cao,² and C. Zhang^{1,*}

¹*School of Engineering Physics, University of Wollongong, New South Wales 2552, Australia*

²*State Key Laboratory of Functional Materials for Informatics, Shanghai Institute of Microsystem and Information Technology, Chinese Academy of Sciences, 865 Changning Road, Shanghai 200050, People's Republic of China*

(Received 26 March 2009; published 10 November 2009)

We reveal that there exists a class of graphene structures (a subclass of bilayer graphene nanoribbons) which has an exceptionally strong optical response in the terahertz (THz) and far infrared (FIR) regime. The peak conductance of THz/FIR active bilayer ribbons is around 2 orders of magnitude higher than the universal conductance of $\sigma_0 = e^2/4\hbar$ observed in graphene sheets. The criterion for the THz/FIR active subclass is a bilayer graphene nanoribbon with a one-dimensional massless Dirac fermion energy dispersion near the Γ point. Our results overcome a significant obstacle that hinders the potential application of graphene in electronics and photonics.

DOI: 10.1103/PhysRevLett.103.207401

PACS numbers: 78.66.Tr, 73.50.Mx, 78.67.-n, 81.05.Uw

In recent years, single layer graphene (SLG) has attracted a great deal of interest [1–4]. New physics has been predicted and observed, such as electron-hole symmetry and the half-integer quantum Hall effect [2,3], finite conductivity at zero charge-carrier concentration [2], and the strong suppression of weak localization [5–7]. Bilayer graphene (BLG) has also attracted considerable attention recently, with seminal experimental and theoretical work being carried out [1,8]. Bilayer calculations use interlayer coupling constants based on the Slonczewski-Weiss-McClure model [9,10]. By further confining the electrons in the graphene plane, one can obtain one-dimensional structures which we refer to as graphene nanoribbons (GNRs) [11]. It has been shown that GNRs with zigzag edges can have finite magnetization with either ferromagnetic order or antiferromagnetic order [12,13]. These properties promise building blocks for technological applications in molecular electronic and optoelectronic devices.

The optical properties of graphene systems is a topic of considerable interest mainly due to universal conductance [14]. The optical conductivity of SLG and bilayer graphene has been calculated [15–18], as has the conductance of various GNRs [19]. All of this research has shown that the optical response of graphene and graphene nanoribbon is extremely weak. In the EM frequency band from terahertz to visible, the absorption coefficient for these systems is generally less than 3% [20–22]. There are two fundamental reasons for this: (1) the density of states vanishes near the Fermi energy, and (2) the interband transition amplitude is small. Because of this, potential application of graphene structures in optoelectronics and photonics is severely limited. To date, these obstacles have remained.

However, we are now able to demonstrate that there exists a subclass of bilayer graphene nanoribbons (BLGNRs) which have an unusually strong optical conductance in the terahertz (THz) to far infrared (FIR) regime. The height of the conductance peak is about 2 orders

of magnitude greater than the universal conductance of graphene sheets. We found that this subclass of BLGNRs can be either armchair or chiral, but their energy dispersion near the Γ point must be that of a one-dimensional massless Dirac fermion. This subclass of graphene structures are the first systems to show such a strong optical response in the absence of any external field in the important frequency band of THz and FIR.

Moreover, it was recently reported that nanoribbons with widths less than 10 nm have been successfully created in the lab [23]. These ribbons were identified as single layer, bilayer, and trilayer ribbons. This remarkable experimental feat demonstrates that, although not yet recognized, the class of structures reported can already be produced.

We first construct a single layer GNR (SLGNR) following the convention of Ezawa [24]; i.e., a ribbon is specified by two indices p and q . We begin by placing $m = p + q$ hexagons next to each other with flat edges touching. On top of this layer, we place an identical layer, offset by q hexagons. Continuing this in both directions we can construct a GNR of arbitrary chirality. Within this model $q = 0$ corresponds to a zigzag (ZZ) edged ribbon, and $q = 1$ corresponds to an armchair (AC) edged ribbon. The number of atoms in the unit cell is given by $N_u = 4q + 2p + 2$. The second layer is now constructed by assuming the standard $A - B$ “Bernal” stacking, along the vertical $C - C$ vector. The net effect is simply shifting the entire second layer up (or down) by an amount $C - C = 1.42 \text{ \AA}$. A typical BLGNR is shown in Fig. 1.

The intralayer coupling is calculated using the tight binding formalism where $\gamma_0 \approx 3 \text{ eV}$ is the nearest neighbor hopping integral. The edge effects of GNRs are incorporated into the tight binding formalism by setting the overlap integral to zero for hopping between edge sites and their neighbors which are off the edge of the ribbon. In this way, the edge states are incorporated into the full electronic properties. The interlayer coupling is restricted to the dominant coupling term $\gamma_1 = 0.36 \text{ eV}$ which occurs

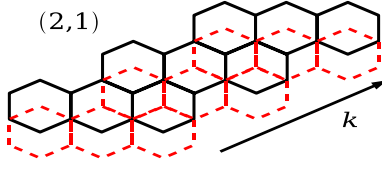


FIG. 1 (color online). The construction of a bilayer graphene nanoribbon. The second layer is identical to the first, but shifted along a $C - C$ vector.

only between A and B sites which sit directly one on top of the other.

We will use the model system of $p = 2$ ribbons, the system with the smallest Hamiltonian matrix, to show the existence of a strong optical conductance peak at low frequencies. Our full numerical result has been obtained for the entire subclass of ribbons. The Hamiltonian matrix for a (2,1) BLGNR is given by

$$H_{(2,1)} = \begin{pmatrix} H_{\text{intra}} & H_{\text{inter}} \\ H_{\text{inter}}^* & H_{\text{intra}} \end{pmatrix}, \quad (1)$$

where the intralayer terms are given by

$$H_{\text{intra}} = \begin{pmatrix} 0 & h \\ h^* & 0 \end{pmatrix} \quad (2)$$

and

$$h = \gamma_0 \begin{pmatrix} h_1 & h_2 & 0 & 0 & 0 \\ h_1^* & h_1 & h_2 & 0 & 0 \\ 0 & h_1^* & h_1 & 0 & h_2 \\ 0 & 0 & h_1^* & h_2 & h_1 \\ 0 & 0 & 0 & h_1 & h_1^* \end{pmatrix}, \quad (3)$$

where $h_1 = e^{ikb\sqrt{3}/2}$ and $h_2 = e^{ikb}$. The interlayer coupling matrix is given by

$$H_{\text{inter}} = \begin{pmatrix} 0 & h' \\ h'^T & 0 \end{pmatrix}, \quad (4)$$

where

$$h' = \begin{pmatrix} 0 & \gamma_1 & 0 & 0 & 0 \\ 0 & 0 & \gamma_1 & 0 & 0 \\ 0 & 0 & 0 & 0 & \gamma_1 \\ 0 & 0 & 0 & \gamma_1 & 0 \\ 0 & 0 & 0 & 0 & 0 \end{pmatrix}. \quad (5)$$

The band structures for ZZ-BLGNRs are shown in Fig. 2(a). They differ from the single layer case as the interlayer coupling produces a second subband corresponding to each single layer subband offset by an amount γ_1 for most of the Brillouin zone. Near the Dirac-like points, however, the intersubband gap goes to zero for the low-energy bands which approach zero energy, and the higher energy bands all approach a degenerate point slightly away from the Dirac-like points. The edge states cause the plateau of the zigzag dispersion at low energies, causing an extended region of zero band gap near the zone boundary. The band structures of AC-BLGNRs shown in

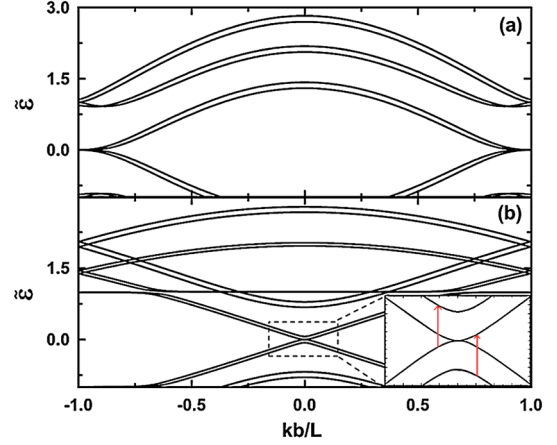


FIG. 2 (color online). The energy dispersion for (a) ZZ-BLGNR and (b) Dirac ZZ-BLGNR. The inset to (b) shows the two sets of symmetric bands near the Dirac point. The arrow represents transitions between nonsymmetric bands which lead to the unusually high optical conductance observed in Fig. 3(b). Here $\tilde{\epsilon} = \epsilon/\gamma_0$.

Fig. 2(b) behave much like 2D bilayer graphene. The linear dispersion at the Dirac points becomes curved, and a second subband appears. Each subband is thus paired. But unlike the ZZ-BLGNR case, the intersubband gap does not go to zero near the Dirac points, but remains as much as $\gamma_1/2$ separated from its pair. As the width increases, this gap approaches zero as the band pairs converge. This is strictly an edge effect, and in the 2D limit a band gap of γ_1 reemerges.

We shall show below that the oscillator strength of the interband transition is strongly dependent on the properties of the energy dispersion at the zero-gap point. It will also be shown that for ZZ-BLGNR, where the zero-gap position is at the K point and the two low-energy dispersions are close to parabolic, the oscillator strength at low energy is very small. On the other hand, for AC-BLGNR, the zero-gap position is at the Γ point. Furthermore, the two low-energy dispersions are very close to linear (or a one-dimensional massless Dirac fermion). Near the band minimum however, the bands are curved, displaying a rounded minimum as opposed to a sharp one. This has two effects: first, it greatly increases the density of states (DOS) at the band minimum, and second, the curvature allows transitions between nonsymmetric bands [shown by an arrow in the inset of Fig. 2(b)]. This effect is identical in all Dirac BLGNRs, which leads to a similar optical response regardless of ribbon width, as we discover below.

The optical conductivity is calculated using the Kubo formula given by

$$\sigma(\omega) = \frac{1}{\omega} \int_0^\infty dt e^{i\omega t} \langle [J(t), J(0)] \rangle, \quad (6)$$

where J , the current operator is given by $\partial H/\partial k_y$. We define the dimensionless photon frequency $\Omega = \hbar\omega/\gamma_0$. In Fig. 3(a) we show that the optical conductivity for the

ZZ-BLGNR exhibits a spike centered on zero energy. This spike occurs here because both low-energy subbands approach zero energy at the Dirac-like points. In the SLGNR case, the velocity operator approaches a constant, which makes inter-symmetric-subband transitions forbidden. This is no longer the case in bilayer ribbons, and there is also now the possibility of low-energy inter-non-symmetric-subband transitions.

Over the full energy spectrum, we see that some of the resonant peaks in the single layer optical conductivity spectrum have split into three peaks. This will not generally be the case. Most peaks will split into two as will be seen in the armchair case. However, near $\Omega = 1$, the subbands create a linear Dirac-like band structure with features similar to the Dirac point in the preceding armchair case, as well as those observed in 2D bilayer graphene. This means that there are three possible energy transitions with high density of states. The central, primary peak corresponds to the original SLGNR peak, and the two secondary peaks, one below, and one above the original by an amount $\Omega = \gamma_1$, correspond to the new curved subbands which do not quite touch the degenerate point from the single layer case.

The optical conductance of armchair BLGNRs is shown in Fig. 3(b). In the AC case it peaks sharply at $\gamma_1/2$ and trails off because of the linearity of the band structure. In the armchair case, a peak is still observed as $\Omega \rightarrow 0$, but the peak at $\gamma_1/2$ is about 2 orders of magnitude stronger. This peak corresponds to vertical transitions between non-symmetric subbands which are far more probable than those between symmetric ones (see Fig. 5 and subsequent discussion). This single low-energy peak is larger than every other peak across the spectrum, and, as can be seen from the inset to Fig. 3(b), is robust across a wide range of relevant temperatures. Of course, the correction due to electron-phonon interactions must be considered with in-

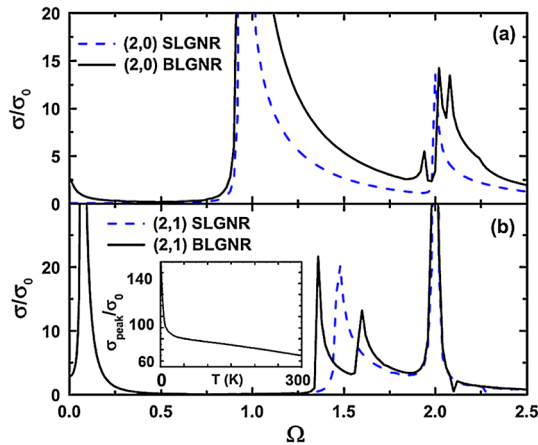


FIG. 3 (color online). The optical conductivity for the ZZ-BLGNR (a) and the AC-BLGNR (b). The low energy optical conductance of the Dirac AC-BLGNR is approximately $150\sigma_0$. The temperature dependence of the large peak observed in all armchair bilayer ribbons is shown in the inset.

creasing temperature. However, the correction at low energies has been found experimentally and deemed negligible, and even for energies >1 eV, to be only a few percent [22]. As the width of the ribbons increases, the strength of this peak remains approximately constant. This is an effect which is peculiar to one-dimensional ribbons, which reflects the consistency of the Dirac band structure with increasing width. In the case of an infinitely wide ribbon, the strong optical response is lost completely, settling at $\approx 4\sigma_0$ at $\Omega = \gamma_1$. This universally enhanced response for arbitrarily wide ribbons is a remarkable result which will certainly be instrumental in abolishing current limitations in implementing graphene-based systems into optoelectronic and photonic devices.

At higher energies, the single peaks observed in AC-SLGNRs generally have split into two, and are separated by an amount $\approx 2\gamma_1$. This corresponds to two sets of symmetric transitions, the nonsymmetric transitions being largely suppressed.

For $q > 1$ BLGNRs, the band gap between the two lowest energy symmetric bands varies from 0 to 1 eV. Similarly the non-Dirac AC-BLGNRs [i.e., $(p+q)/3 \notin \mathbb{Z}$], have varying band gaps for the lowest energy subbands.

For a given type of BLGNR, the conductance peak position can be tuned with the ribbon width. Figure 4 shows the width dependence of the peak position in the THz/FIR regime. The peak position oscillates with the ribbon width. The amplitude of the oscillation is of the same order of magnitude as the average peak position, indicating a large range for tuning the resonance peak. The period of the oscillation increases with the chirality (q). The inset of Fig. 4 shows the width dependence of the energy gap for Dirac BLGNRs. This gap decreases as width increases making the location of the optical peak strongly width dependent. The strength of the peak, however, remains constant as discussed earlier. This makes

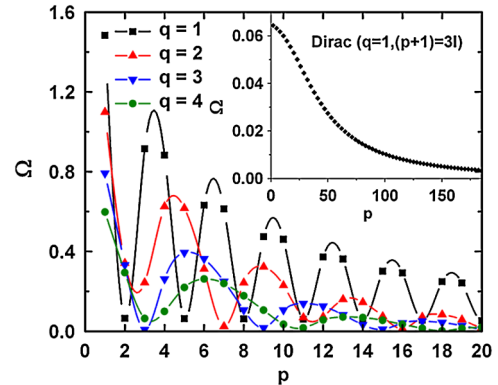


FIG. 4 (color online). The width dependence of the energy of the low-energy peak for BLGNRs with $q = [1, 4]$. The strongest peaks occur in the lowest energy gaps in the Dirac armchair ribbons. The inset shows the width dependence of the band gap for Dirac BLGNRs with strong low energy optical response. This gap eventually disappears, but in the 2D limit with no edges, it reemerges at γ_1 .

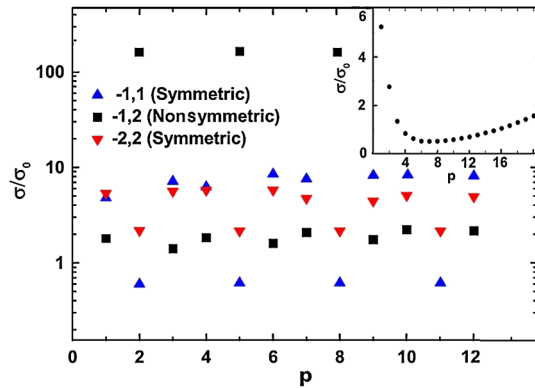


FIG. 5 (color online). The p dependence of the low-energy peaks for a $(p,1)$ BLG NR. The peak strength in the Dirac cases is constant within the numerical accuracy. Inset: The width dependence of the magnitude of the low energy peak for the ZZ-BLG NRs decreases quickly with increasing width, and then increases steadily for $p > 6$.

Dirac bilayer graphene nanoribbons remarkably versatile in choosing the desired optical response energy without compromising on response strength. The bilayer ribbons that have recently been fabricated [23] correspond to $p < 100$ in our results. Furthermore, energy gaps in the THz regime correspond to bilayer ribbons with $p \geq 100$. This demonstrates that the structures in question already exist, and the gateway to graphene-based THz devices is extremely close.

Figure 5 shows the width dependence of the magnitude of the low-energy peak for the $(p, 1)$ BLG NR. For $(p + 1)/3 \in I$, the nonsymmetric matrix element dominates, causing the single low-energy peak. The low-frequency peak conductance for this class of BLG NRs is unusually strong having a value of approximately $150\sigma_0$, much stronger than the universal conductance of graphene sheets [22]. When the Dirac condition is not met, however [i.e., $(p + 1)/3 \notin I$], the symmetric matrix elements dominate, and the nonsymmetric matrix elements are greatly suppressed, leading to a much weaker response to the low-energy spectrum. The inset of Fig. 5 shows the width dependence of the strength of the low-energy peak for ZZ-BLG NRs. For $p > 6$ as the width increases, the low-energy subbands remain lower, which increases the DOS, allowing more transitions between subbands. For very narrow width ZZ-BLG NRs however, the curvature in the subbands is so high that the velocity operator allows strong coupling between the subbands, which makes the low-energy magnitude very strong.

In summary, we have shown that the interplay of ribbon's chirality and the inter-ribbon coupling can lead to significant enhancement in optical response. We have identified a subclass of BLG NRs where the interlayer coupling causes a finite band gap in the energy minimum and induces strong intersubband transitions. The peak conductance of this class of BLG NRs has a very large constant value of around $150\sigma_0$, making them a class of materials

for unique applications in optoelectronics. The simple picture behind this phenomenon is that the density of states for the 1D massless Dirac fermions remains finite at zero energy, whereas that for the 2D massless Dirac fermions in a graphene sheet vanishes. The remarkable role of the edge states is to cause the transition energy to decrease with increasing width, but not the magnitude of response. In the 2D limit, however, with edge states removed, the strong optical response suddenly disappears completely.

These results open a gateway to the creation of graphene-based low-energy photon devices. The ribbon width and chirality selection for various applications is crucial, as the optical responses of various ribbons change dramatically when these properties are varied.

This work is supported by the Australian Research Council, the 973 Program of China (2007CB310402), the major project and Hundred Scholar Plan of CAS.

*czhang@uow.edu.au

- [1] K. S. Novoselov *et al.*, *Science* **306**, 666 (2004).
- [2] K. S. Novoselov *et al.*, *Nature (London)* **438**, 197 (2005).
- [3] Y. Zhang, Y. W. Tan, H. L. Stormer, and P. Kim, *Nature (London)* **438**, 201 (2005).
- [4] C. Berger *et al.*, *Science* **312**, 1191 (2006).
- [5] H. Suzuura and T. Ando, *Phys. Rev. Lett.* **89**, 266603 (2002).
- [6] S. V. Morozov *et al.*, *Phys. Rev. Lett.* **97**, 016801 (2006).
- [7] D. V. Khveshchenko, *Phys. Rev. Lett.* **97**, 036802 (2006).
- [8] E. McCann and V. I. Fal'ko, *Phys. Rev. Lett.* **96**, 086805 (2006).
- [9] J. C. Slonczewski and P. R. Weiss, *Phys. Rev.* **109**, 272 (1958).
- [10] J. W. McClure, *Phys. Rev.* **108**, 612 (1957).
- [11] Y. W. Son, M. L. Cohen, and S. G. Louie, *Phys. Rev. Lett.* **97**, 216803 (2006).
- [12] Y. W. Son, M. L. Cohen, and S. G. Louie, *Nature (London)* **444**, 347 (2006).
- [13] Q. Yan *et al.*, *Nano Lett.* **7**, 1469 (2007).
- [14] E. Fradkin, *Phys. Rev. B* **33**, 3263 (1986).
- [15] C. Zhang, L. Chen, and Z. Ma, *Phys. Rev. B* **77**, 241402 (R) (2008).
- [16] T. Stauber, N. M. R. Peres, and A. K. Geim, *Phys. Rev. B* **78**, 085432 (2008).
- [17] J. Cserti, A. Csordas, and G. David, *Phys. Rev. Lett.* **99**, 066802 (2007).
- [18] A. R. Wright, F. Liu, and C. Zhang, *Nanotechnology* **20**, 405203 (2009).
- [19] J. Liu, A. R. Wright, C. Zhang, and Z. Ma, *Appl. Phys. Lett.* **93**, 041106 (2008).
- [20] V. P. Gusynin, S. G. Shrapov, and J. P. Carbotte, *Phys. Rev. Lett.* **96**, 256802 (2006).
- [21] A. B. Kuzmenko, E. van Heumen, F. Carbone, and D. van der Marel, *Phys. Rev. Lett.* **100**, 117401 (2008).
- [22] R. R. Nair *et al.*, *Science* **320**, 1308 (2008).
- [23] X. Li, X. Wang, L. Zhang, S. Lee, and H. Dai, *Science* **319**, 1229 (2008).
- [24] M. Ezawa, *Phys. Rev. B* **73**, 045432 (2006).